

# Study of the Bulk Magnetic and Electrical Properties of $\text{MgFe}_2\text{O}_4$ Synthesized by Chemical Method

Sheikh Manjura Hoque<sup>1</sup>, M. Abdul Hakim<sup>1</sup>, Al Mamun<sup>1</sup>, Shireen Akhter<sup>1</sup>, Md. Tanvir Hasan<sup>2</sup>, Deba Prasad Paul<sup>2</sup>, Kamanio Chattopadhyay<sup>3</sup>

<sup>1</sup>Materials Science Division, Atomic Energy Centre, Dhaka, Bangladesh; <sup>2</sup>Department of Physics, Chittagong University, Chittagong, Bangladesh; <sup>3</sup>Department of Materials Engineering, Indian Institute of Science, Bangalore, India.  
Email: manjura\_hoque@yahoo.com

Received June 30<sup>th</sup>, 2011; revised August 12<sup>th</sup>, 2011; accepted August 27<sup>th</sup>, 2011.

## ABSTRACT

Nanocrystalline Magnesium ferrite has been prepared by chemical co-precipitation technique. Structural characterization has been performed by X-ray diffraction. Formation of ferrites has also been studied by using FTIR. Frequency dependence of real and imaginary part of initial permeability has been presented for the samples sintered at different temperatures. Real part of initial permeability, increases with the increase of grain growth. The loss component represented by imaginary part of initial permeability decreases with frequency up to the measured frequency of this study of 13 MHz. Curie temperatures have been determined from the temperature dependence of permeability. Curie temperatures for the samples of this composition do not vary significantly with the variation of sintering temperatures. B-H loop measurements have been carried out by B-H loop tracer. Transport property measurements haven been carried out by electrometer and impedance analyzer.

**Keywords:**  $\text{MgFe}_2\text{O}_4$ , Nanograins, Complex Initial Permeability, B-H Curves, Transport Properties

## 1. Introduction

Magnesium ferrite ( $\text{MgFe}_2\text{O}_4$ ) is an important magnetic oxide with spinel structure. Magnesium ferrite and allied compounds have found wide spread applications in microwave device because of their low magnetic and dielectric losses and high resistivity.  $\text{MgFe}_2\text{O}_4$  enjoys special attention for microwave application such as circulators, insulator and phase shifters [1]. Magnesium ferrite is also used in high-density recording media, heterogeneous catalysis and sensors.  $\text{MgFe}_2\text{O}_4$  is also known for its good photoelectric effect [2-4]. Synthesis of  $\text{MgFe}_2\text{O}_4$  nanoparticle has been attempted by several investigators [5-8]. Rane *et al.* [9] have studied dielectric behavior of  $\text{MgFe}_2\text{O}_4$  prepared from chemically beneficiated iron ore rejects and have arrived at the conclusion that chemically beneficiated iron ore rejects can, hence, be effectively used in the synthesis of high quality ferrites. Candeia *et al.* [10] have studied  $\text{MgFe}_2\text{O}_4$  pigment obtained at low temperature by polymeric precursor method. Doroftei *et al.* [11] have studied microstructure and humidity sensitive properties of  $\text{MgFe}_2\text{O}_4$  ferrite with Sn and Mo sub-

stitutions prepared by self-combustion method. Gateshki *et al.* [12] have studied structure of nanocrystalline  $\text{MgFe}_2\text{O}_4$  from X-ray diffraction, Rietveld and atomic pair distribution function analysis. Though numbers of research papers are available in the literature on  $\text{MgFe}_2\text{O}_4$ , synthesis of nanoferrites by chemical method is still considered to be in the infancy state in terms of reproducibility and further improvement.

$\text{MgFe}_2\text{O}_4$  is known for its ideal mixed-spinel structure consists of a face-centered cubic close-packed oxygen sublattice in which a fraction of the tetrahedral (T) and octahedral (O) sites are filled by Mg ions. The crystal structure of spinel ferrites can be formulated in greater detail as  $(\text{Mg}_{1-\delta}\text{Fe}_\delta)[\text{Mg}_\delta\text{Fe}_{2-\delta}]\text{O}_4$ . The parentheses and the square brackets denote cation sites of fourfold (T) and sixfold [O] oxygen coordination, respectively where,  $\delta$  represents the so-called degree of inversion (defined either as the fraction of the (T) sites occupied by  $\text{Fe}^{3+}$  cations or as the fraction of the [O] sites occupied by  $\text{Mg}^{2+}$  cations. It is widely known that since  $\text{Mg}^{+2}$  is non-magnetic, magnetic moment of  $\text{MgFe}_2\text{O}_4$  is derived from

the particular type of cation distribution. The cation distribution in spinel ferrites upon which many physical and chemical properties depend, is a complex function of processing parameters. It is an established fact that there is a remarkable effect of initial particle size on bulk properties of sintered product. Further chemically synthesized particles contain lesser amount of impurity and higher surface to volume ratio. Conventionally, sintering temperature of  $\text{MgFe}_2\text{O}_4$  is very high. There is a possibility of reducing the sintering temperature of technologically important  $\text{MgFe}_2\text{O}_4$  to attain optimum properties and thus reduce processing cost. The purpose of the present study is to investigate the effect of nanosized particle as starting material on bulk properties of  $\text{MgFe}_2\text{O}_4$  sintered at various temperatures.

## 2. Experimental

We have used a standard co-precipitation technique to produce fine particles of  $\text{MgFe}_2\text{O}_4$ . The analytical grade of  $\text{Fe}(\text{NO}_3)_3 \cdot 9\text{H}_2\text{O}$ ,  $\text{Mg}(\text{NO}_3)_2 \cdot 6\text{H}_2\text{O}$  and  $\text{NaOH}$  were mixed in required molar ratio and added to 8 M  $\text{NaOH}$  solution with constant stirring at room temperature. The precipitate was heated to  $80^\circ\text{C}$  with constant stirring. When reaction was completed the precipitate was centrifuged at 15,000 rpm for 20 minutes, then washed and filtered for 10 times with distilled water. Finally, the precipitate was heated at  $90^\circ\text{C}$  for 36 hours. The powder was pelletized and sintered at various temperatures in the range of  $200^\circ\text{C}$  -  $1400^\circ\text{C}$ . Formation of ferrites has been studied by X-ray diffraction and also by FTIR. Microstructure has been studied using scanning electron microscope. Complex initial permeability and dielectric constants have been measured by using impedance analyzer. B-H loops were studied using B-H loop tracer. Temperature dependence of resistivity has been studied by electrometer and laboratory built furnace.

## 3. Results and Discussion

In **Figure 1**, X-ray diffraction patterns of samples calcined in the range of  $500^\circ\text{C}$  to  $1000^\circ\text{C}$  for 3 hours have been presented. The curves reveal decrease of FWHM with the increase of sintering temperature. The grain size has been obtained from Scherrer's formula using Full Width Half Maxima (FWHM) and peak position of the sample after correcting instrumental broadening and presented in **Figure 2**. The grain size was estimated to be around 21 nm for the sample sintered at  $500^\circ\text{C}$ . With the increase of sintering temperature the grain size increases dramatically and reached the value of around 75 nm for the sample sintered at  $1000^\circ\text{C}$ . For the further increase of sintering temperature of around  $1200^\circ\text{C}$  -  $1400^\circ\text{C}$ , it was not possible to measure grain size with X-ray diffraction since instrumental broadening at this point was compar-

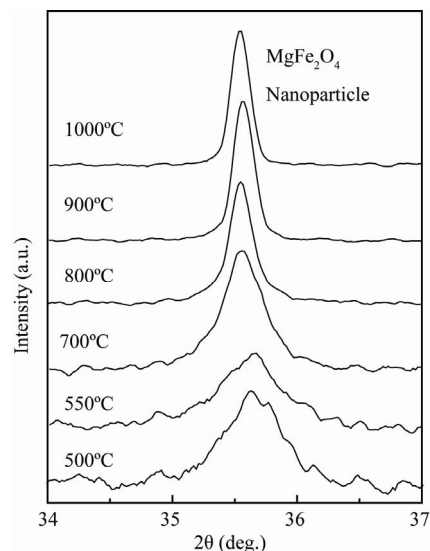


**Figure 1.** X-ray diffraction patterns of  $\text{MgFe}_2\text{O}_4$  for the samples sintered at different temperatures for 3 hr.

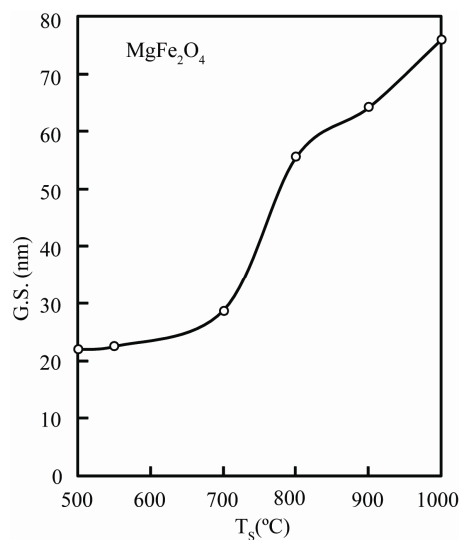


**Figure 2.** Variation of grain size with sintering temperature for 3 hr of sintering time.

ble to the value of FWHM.

The variation of lattice parameter with sintering temperature has been presented in **Figure 3**. The variation in lattice parameter for the sample prepared from nanograins has been studied by several investigators [13,14]. Hankare *et al.* has reported the value of lattice parameter as  $8.33 \text{ \AA}$  [13] while Sattar *et al.* has found lattice parameter higher than the standard JCPDS data [14]. The lattice parameter increases sharply during sintering upto  $700^\circ\text{C}$ . No change in lattice parameter can be detected beyond this temperature indicating completion of ferritization. This corresponds to sintered grain size of 26 nm.

In **Figure 4**, X-ray diffraction pattern of  $\text{MgFe}_2\text{O}_4$  sin-

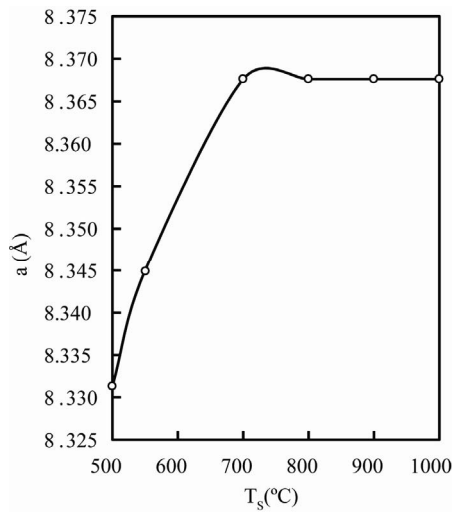


**Figure 3.** Variation of lattice parameter with sintering temperature for 3 hr sintering time.

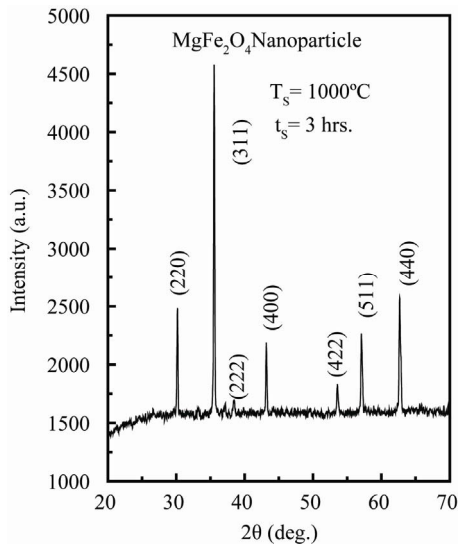


**Figure 4.** X-ray diffraction pattern of  $\text{MgFe}_2\text{O}_4$  for the sintering temperature of  $1000^\circ\text{C}$  for 3 hr.

tered at  $1000^\circ\text{C}$  has been presented. All the peaks were indexed in terms of the known structure of  $\text{MgFe}_2\text{O}_4$ . Lattice parameter reached a reported value of  $8.367 \text{ \AA}$  at  $1000^\circ\text{C}$ , which is close to the reported equilibrium value for  $\text{MgFe}_2\text{O}_4$  *i.e.*  $8.376 \text{ \AA}$ .

The FTIR spectra of  $\text{MgFe}_2\text{O}_4$  nanoparticle sample in the range  $1000 - 350 \text{ cm}^{-1}$  is shown for the samples sintered in the range of  $1200^\circ\text{C} - 1400^\circ\text{C}$  in **Figure 5**. In the FTIR spectrum of  $\text{MgFe}_2\text{O}_4$  in the range  $1000 - 350 \text{ cm}^{-1}$  absorption bands correspond to the vibration of tetrahedral and octahedral complexes at  $\nu_1 \sim 572 \text{ cm}^{-1}$  and  $\nu_2 \sim 409 \text{ cm}^{-1}$  at  $1200^\circ\text{C}$  respectively, which is indicative of the formation of spinel ferrite structure. The presence of long shoulder for the A and B site is indicative of the

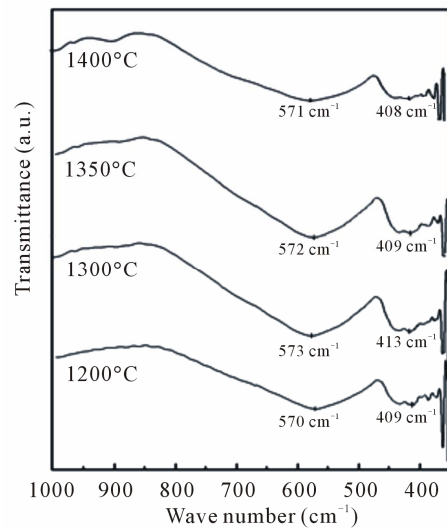


**Figure 5.** FTIR spectra of  $\text{MgFe}_2\text{O}_4$  sintered at different temperatures.

presence of different ionic states in that site. It is seen from the FTIR data that the normal mode of vibration of tetrahedral cluster is higher than that of octahedral cluster. This can be due to the shorter bond length of tetrahedral cluster than the octahedral cluster. It can be noted that the value of  $\nu_1$  and  $\nu_2$  remain almost unchanged with the sintering temperature. This indicates that there is very little change of cation distribution with the increase of sintering temperature in the range of  $1200^\circ\text{C}$  to  $1400^\circ\text{C}$ . It will be seen later that there is almost no change in Curie temperature with the increase of sintering temperature, which further indicate that there is very little or no change of cation distribution.

SEM microstructure of the samples of  $\text{MgFe}_2\text{O}_4$  sintered at  $1250^\circ\text{C}$ ,  $1350^\circ\text{C}$  and  $1400^\circ\text{C}$  has been presented in **Figure 6** with the magnification of  $\times 3000$ . Calculated grain size for  $\text{MgFe}_2\text{O}_4$  has been obtained as 4, 5 and  $10 \mu\text{m}$  for the samples sintered at  $1250^\circ\text{C}$ ,  $1350^\circ\text{C}$  and  $1400^\circ\text{C}$  respectively. It can be observed from the figure that the grain size of the sample sintered at  $1250^\circ\text{C}$  is smaller. With the increase of sintering temperature, microstructure becomes more homogeneous in association with an increase of grain size. Further, considerable amount of pores can be seen in the microstructure of sample sintered at  $1250^\circ\text{C}$ . Amount of pores decrease with the increase of sintering temperature.

Frequency stability of  $\mu'$  is an important criteria of soft magnetic materials for its application in microwave devices. The general characteristic of frequency spectrum of permeability curves is  $\mu'$  remains fairly constant up to some critical frequency beyond which  $\mu'$  decreases characterized by the onset resonance of loss governed by Snoek's law. At critical frequency  $\mu'$  drops rapidly.

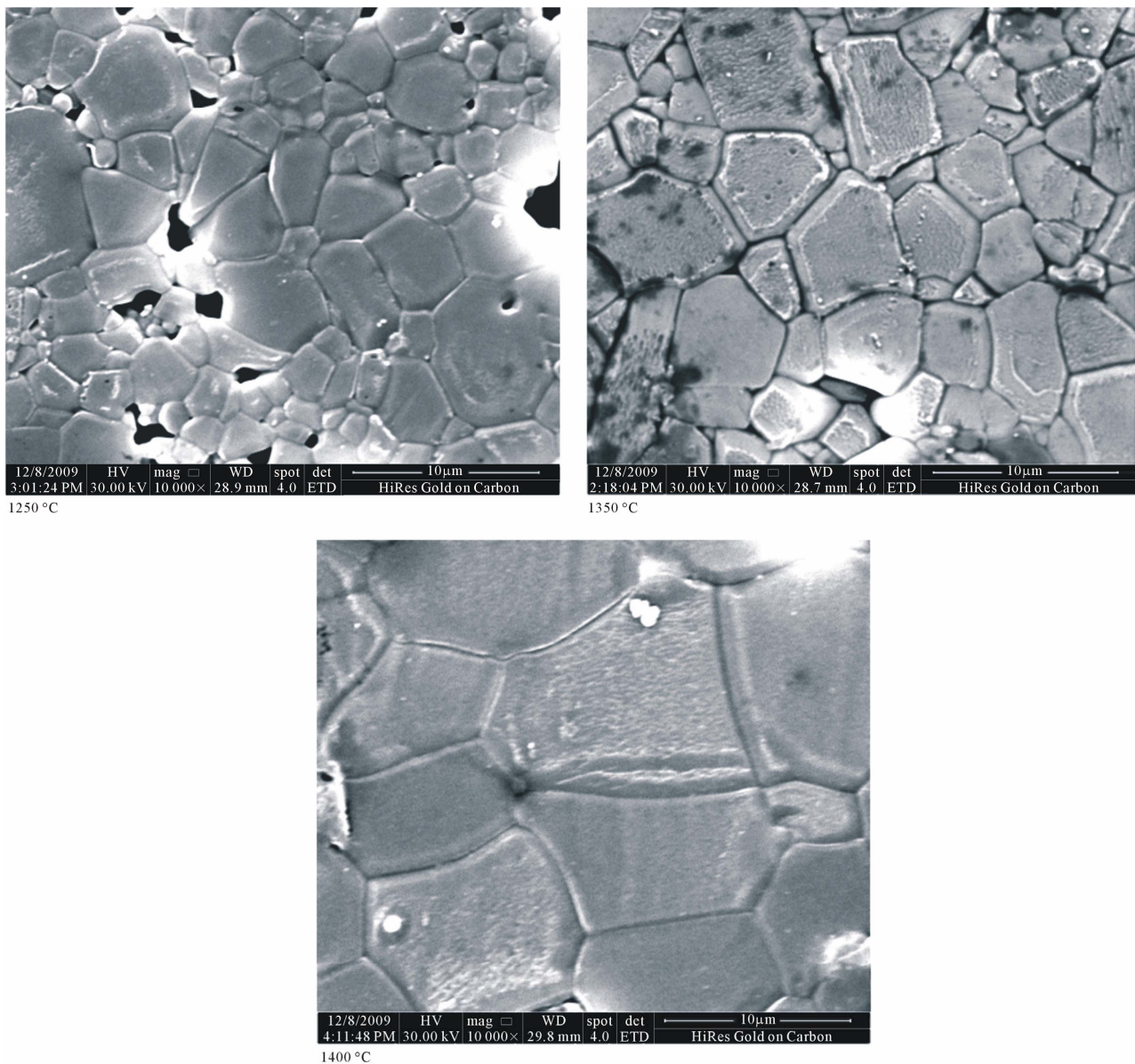


**Figure 6.** SEM micrographs for the samples sintered at 1250°C, 1350°C and 1400°C for 3 hr.

The nature of these curves and critical frequency at which onset of resonance takes place depend on the ionic states of cations, density and grain size. The permeability generally increases with the increase of grain size. The presence of small grain size interferes with wall motion, which decreases both real and imaginary part of permeability and increases stability region of  $\mu'$ . At higher frequencies, losses are found to be lower if domain wall motion is inhibited and the magnetization is forced to change by rotation.

**Figure 7** shows frequency spectrum of real part of initial permeability  $\mu'$  at various sintering temperatures.  $\mu'$  increases with the increase of sintering temperature be-

cause of the increase of grain size and densification. At higher sintering temperatures inhibition of domain wall mobility decreases to a great extent, which leads to the increase of  $\mu'$ . In **Figure 8**, frequency spectrums of imaginary part of initial permeability  $\mu''$  are presented at different sintering temperature. The low frequency value of  $\mu''$  increases with the increase of sintering temperature due to lower inhibition of domain wall motion. This also increases natural frequency of precession, which absorbs more energy leading to enhancement of losses. Frequency responses of both real and imaginary part of permeability for the samples of this study are characterized by high degree of stability which is suitable for microwave

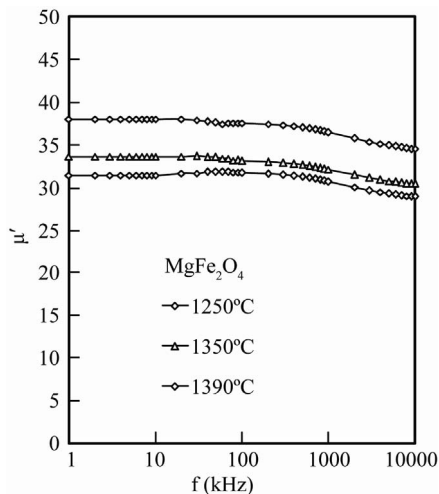


**Figure 7.** Frequency dependence of real and imaginary part of initial permeability ( $\mu'$  and  $\mu''$ ) for the samples sintered at 1250°C, 1350°C and 1400°C.

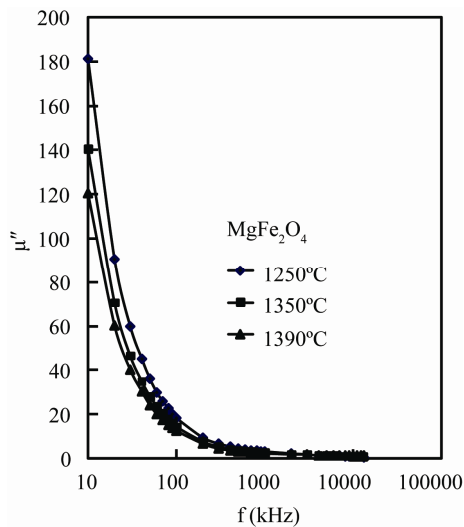


**Figure 8.** Temperature dependence of initial permeability  $\mu'$  for the samples sintered at 1250°C, 1350°C and 1400°C.

applications.

Curie temperature measurement involves the measurement of permeability  $\mu'$  varying with temperature. In **Figure 9**, temperature dependence of permeability of samples obtained at various sintering temperature of 1250°C, 1350°C, 1400°C for 3 hrs are presented. At Curie temperature  $T_c$ , complete spin disorder takes place. The sharpness of the fall of  $\mu'$  at  $T_c$  indicates the homogeneity of the studied samples. From **Figure 9**, it can be observed that the Curie temperature does not vary with sintering temperature. This complies with intrinsic nature of Curie temperature, which does not vary with grain size and porosity. Invariance of Curie temperature with sintering temperature also implies that there is little or no

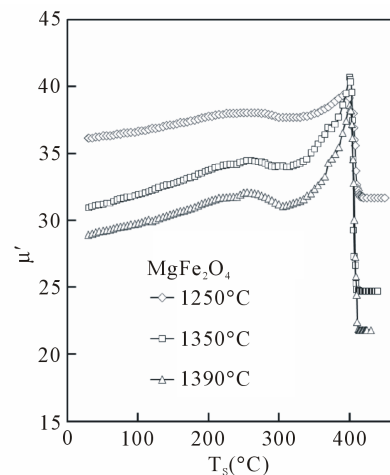


**Figure 9.** Temperature dependence of initial permeability  $\mu'$  for the samples sintered at 1250°C, 1350°C and 1400°C.

change of cation distribution in the sintering temperature range of 1200°C - 1400°C in compliance with the results obtained from FTIR presented in **Figure 5**.

In **Figure 10**, primary induction curves of  $\text{MgFe}_2\text{O}_4$  of the samples sintered at 1250°C, 1350°C and 1400°C for 3 hr have been presented. The curves are characterized by the pinning effect of the domain wall movement. This is due to the presence of increased number of pores and also because of smaller grain size, which leads to increased volume fraction of grain boundary. Both the pores and grain boundaries inhibit domain wall movement. With the increase of sintering temperatures, pores and grain boundary effects are reduced due to higher densification and grain growth. This is manifested in the initial part of primary induction curve known as Rayleigh region where lower field is required to achieve higher magnetization due to the elimination of more number of defects in the sample with progressive increase of sintering temperatures.

In **Figure 11**, B-H hysteresis graphs of the sintered samples are presented. In **Figure 12**, coercivity, remanent ratio and core loss derived from **Figure 11** are presented. From both the figures, it may be observed that the coercivity and remanent ratio decrease with the increase of sintering temperature. This is typically valid for extrinsic properties, which depends on grain size and porosity of the samples. Core loss, which is mainly related to the area of the hysteresis loops decrease with the increase of sintering temperature. More importantly, it might be noticed the shape of the B-H curves, which possess higher squareness ratio. Maximum remanent ratio is around 0.8.

In order to attain high remanent ratio in polycrystalline ferrites, several general conditions must be fulfilled [15]. First of all, they should have a high degree of symmetry

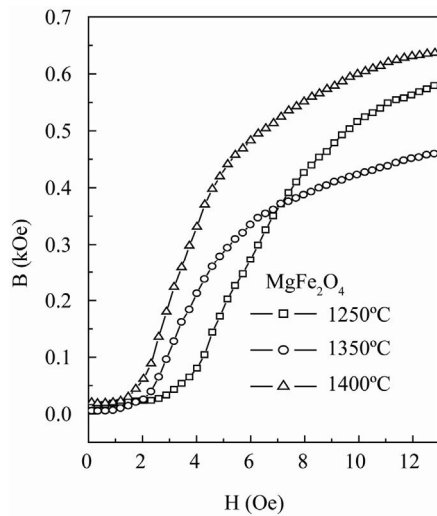


**Figure 10.** Primary induction curves of  $\text{MgFe}_2\text{O}_4$  for the samples sintered at 1250°C, 1350°C and 1400°C.

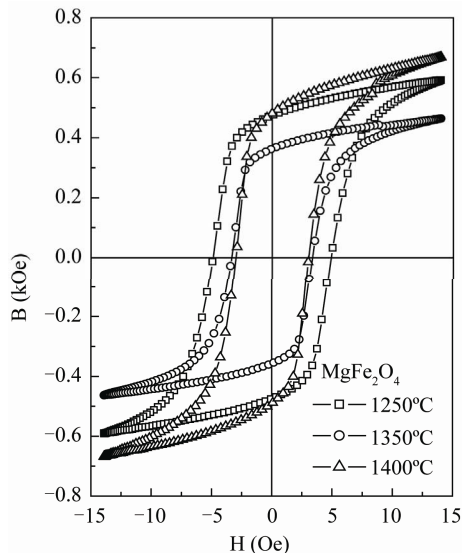


**Figure 11.** B-H hysteresis loops of  $\text{MgFe}_2\text{O}_4$  for the samples sintered at 1250°C, 1350°C and 1400°C.

(magnetic homogeneity), *i.e.*, their structure should have as many directions of easy magnetization as possible. This condition is realized more closely in ferrites with a cubic lattice structure and a negative  $K_1$  constant. Secondly, crystallographic anisotropy should predominate over other types of anisotropy (shape, stress). This means a need for low internal stresses, magnetostriction, and porosity as well as high homogeneity of the material. In this case the ratio  $\sqrt{K_1/M_S}$  ( $M_S$  is the saturation magnetization) should be rather high. Thirdly, magnetic coupling between grains, determined by the ratio  $M_S^2/K_1$ , should be strong. The second and third conditions impose contradictory requirements on the values of  $K_1$  and  $M_S$ . Con-

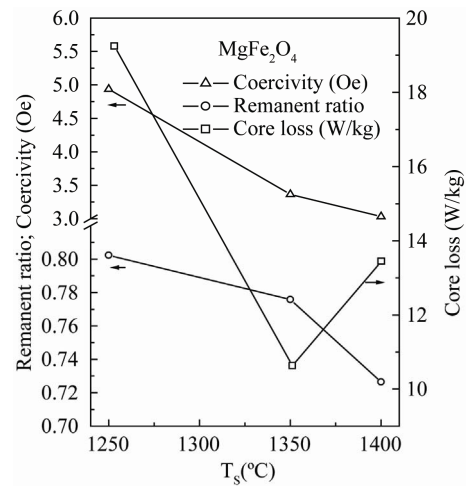


**Figure 12.** Sintering temperature dependence of Coercivity, Remanent ratio and Core loss.

sequently, ferrites will have a rectangular hysteresis loop only if they have compositions for which the values of  $K_1$ ,  $M_S$  lie within a certain range. Such ferrospones should have the required homogeneity of the residual porosity and grains. They should also include microscopic inhomogeneities which are required for forming domains of reverse magnetization or restraining the motion of the boundaries of such domains before a field of certain strength is applied.

In **Figure 13**, dc resistivity data as a function of inverse temperature have been presented. Room temperature resistivity for all the samples sintered in the range of 1250°C - 1400°C is more than around  $\sim 10^6 \Omega \text{ cm}$ . The resistivity decreases with increasing sintering temperatures. The value of  $\rho$  is the lowest for the samples sintered at 1400°C. When polycrystalline ferrites are considered, the bulk resistivity arises from a combination of crystallite resistivity and the resistivity of crystallite boundaries. The boundary resistivity is much greater than that of the crystallite resistivity. Thus the boundary has the greatest influence on the dc resistivity. The decrease of resistivity is also related to the decrease of porosity at higher sintering temperature since pores are non-conductive, which increases resistivity of the material. The resistivity increases with the increase of porosity at lower sintering temperature because charge carriers on their way face the pores. The activation energy decreases with increasing sintering temperature. Decrease of activation energy with the increase of sintering temperatures may be attributed to the fact that at a high sintering temperature, partial reduction of  $\text{Fe}^{3+}$  to  $\text{Fe}^{2+}$  takes place locally and these places act as donor centre. The conduction mechanism is due to hopping of electrons of the type  $\text{Fe}^{2+} \leftrightarrow \text{Fe}^{3+}$ .

The dielectric constants of the ferrites in the form of pellets were determined using LCR circuit. The variation of real and imaginary part of dielectric constant ( $\epsilon'$  and  $\epsilon''$ ) as a function of frequency for MgFe<sub>2</sub>O<sub>4</sub> for various sintering temperatures are shown in **Figures 14** and **15**. From **Figure 14**, dispersion in dielectric constants can be observed for all the samples sintered at various temperatures. To explain the dielectric dispersion in ferrites, grain and grain boundaries were assumed to be two different layers each having the same dielectric constant. As the frequency rises from a low value the bulk resistivity  $\rho$  and dielectric constant  $\epsilon'$  fall and become asymptotic to lower values at higher frequencies. This variation has the characteristic of relaxation and is attributed to the granular structure of ferrites, in which crystallites are separated

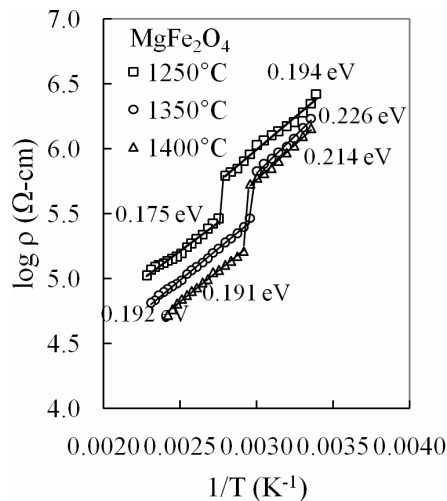


**Figure 13.** Temperature dependence of resistivity  $\rho$  for the samples sintered at 1250°C, 1350°C and 1400°C.

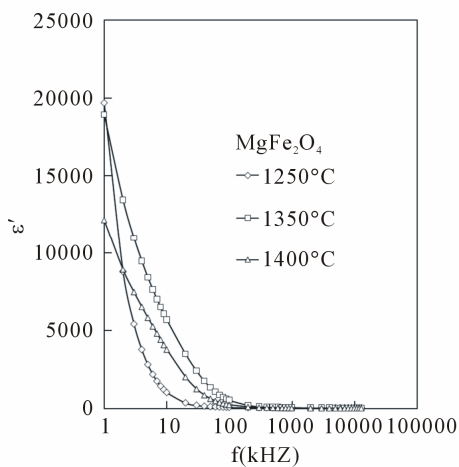


**Figure 14.** Frequency dependence of real part dielectric constant  $\epsilon'$  for the samples sintered at 1250°C, 1350°C and 1400°C.

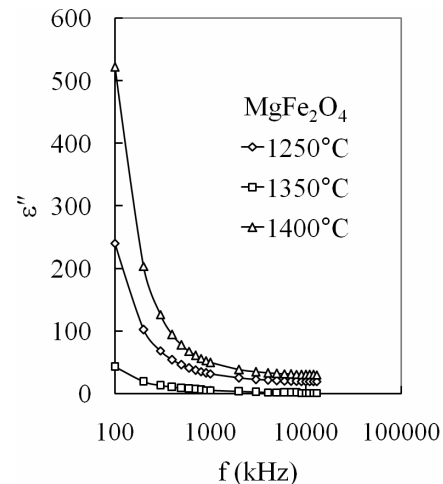


**Figure 15.** Frequency dependence of imaginary part dielectric constant  $\epsilon''$  for the samples sintered at 1250°C, 1350°C and 1400°C.

by boundaries having much higher resistivity than the crystallites. Thus the structure behaves as a compound dielectric. At low frequencies the impedance of the crystallites are negligible compared to that of the boundary.

The dielectric constant approaches to the value, which is analogous to calculating dielectric properties from measurements on a specimen between the plates of capacitor, using a dielectric length  $1/n$  times the actual value. At very high frequencies the boundary capacitance becomes short circuited with the boundary resistance and the bulk dielectric properties approach those of crystallites. Real part of dielectric constant exhibits rapid increase with decrease of frequency. The imaginary part of dielectric constant increase much more slowly compared to usual values of  $\epsilon''$  for ferrites. **Figure 15** shows no extra peak, because of high bulk resistivity.

#### 4. Conclusions

Nanocrystalline MgFe<sub>2</sub>O<sub>4</sub> has been prepared by chemical co-precipitation technique and sintered at different temperatures. The particle size has been obtained from Scherrer's formula and found around 26 nm at 700°C where single phase MgFe<sub>2</sub>O<sub>4</sub> has formed. When the samples were calcined at higher temperatures subsequent grain growth has taken place. Further calcinations at 1000°C led to the grain size of 75 nm. SEM micrographs reveal increase in grain size with increasing sintering temperatures along with significant decrease of pores. Curie temperature remains unchanged with the increase of sintering temperature. The B-H loops are characterized by higher squareness ratio, the maximum value of which is around 0.8. The resistivity decreases with the increase of sintering temperature. The decrease of resistivity is re-

lated to the increase of grain size and decreasing porosity since pores are non conductive, which increases the resistivity of the material. The highest values of dielectric constant ( $\epsilon'$ ) can be observed for the samples having lower resistivity. Dispersion in dielectric constant is observed for all the samples at lower frequency.

## 5. Acknowledgements

The authors acknowledge with great appreciation, the support provided by Ministry of Science, Information and Communication Technology, Government of People's Republic of Bangladesh, Bangladesh Atomic Energy Commission and International Science Program, Uppsala University, Sweden.

## REFERENCES

- [1] D. Bahadur, "Current Trends in Applications of Magnetic Ceramic Materials," *Bulletin of Materials Science*, Vol. 15, No. 5, 1992, pp. 431-439. [doi:10.1007/BF02745292](https://doi.org/10.1007/BF02745292)
- [2] R. J. Wiley, P. Noirclere and G. Busca, "Preparation and Characterization of Magnesium Chromite and Magnesium Ferrite Aerogel," *Chemical Engineering Communication*, Vol. 123, No. 1, 1993, pp. 1-17. [doi:10.1080/00986449308936161](https://doi.org/10.1080/00986449308936161)
- [3] L. G. J. de Haart and G. Blasse, "Photoelectrochemical Properties of Ferrites with the Spinel Structure," *Solid State Ionics*, Vol. 16, 1985, pp. 137-139. [doi:10.1016/0167-2738\(85\)90035-9](https://doi.org/10.1016/0167-2738(85)90035-9)
- [4] Y. Huang, Y. Tang, J. Wang and Q. Chen, "Synthesis of MgFe<sub>2</sub>O<sub>4</sub> Nanocrystallites under Mild Conditions," *Materials Chemistry and Physics*, Vol. 97, No. 2-3, 2006, pp. 394-397. [doi:10.1016/j.matchemphys.2005.08.035](https://doi.org/10.1016/j.matchemphys.2005.08.035)
- [5] S. K. Pradhan, S. Bid, M. Gateshki and V. Petkov, "Micro-Structure Characterization and Cation Distribution of Nanocrystalline Magnesium Ferrite Prepared by Ball Milling," *Materials Chemistry and Physics*, Vol. 93, No. 1, 2006, pp. 224-230. [doi:10.1016/j.matchemphys.2005.03.017](https://doi.org/10.1016/j.matchemphys.2005.03.017)
- [6] S. Verma, P. A. Roy, Y. B. Kholam, H. S. Potdar and S. B. Deshpande, "Synthesis of Nanosized MgFe<sub>2</sub>O<sub>4</sub> Powders by Microwave Hydrothermal Method," *Materials Letters*, Vol. 58, No. 6, 2004, pp. 1092-1095. [doi:10.1016/j.matlet.2003.08.025](https://doi.org/10.1016/j.matlet.2003.08.025)
- [7] M. Rashad, "Magnetic Properties of Nanocrystalline Magnesium Ferrite by Co-Precipitation Assisted with Ultrasound Irradiation," *Journal of Materials Science*, Vol. 42, No. 13, 2007, pp. 5248-5255. [doi:10.1007/s10853-006-0389-9](https://doi.org/10.1007/s10853-006-0389-9)
- [8] A. Pradeep and G. Chandrasekaran, "FTIR Study of Ni, Cu and Zn Substituted Nano-Particles of MgFe<sub>2</sub>O<sub>4</sub>," *Materials Letters*, Vol. 60, No. 3, 2006, pp. 371-374. [doi:10.1016/j.matlet.2005.08.053](https://doi.org/10.1016/j.matlet.2005.08.053)
- [9] K. S. Rane, V. M. S. Verenkar and P. Y. Sawant, "Dielectric Behaviour of MgFe<sub>2</sub>O<sub>4</sub> Prepared from Chemically Beneficiated Iron Ore Rejects," *Bulletin of Materials Science*, Vol. 24, No. 3, 2000, pp. 323-330. [doi:10.1007/BF02704930](https://doi.org/10.1007/BF02704930)
- [10] R. A. Candeia, M. A. F. Souza, M. I. B. Bernardi, S. C. Maestrelli, I. M. G. Santos, A. G. Souza and E. Longo, "MgFe<sub>2</sub>O<sub>4</sub> Pigment Obtained at Low Temperature," *Materials Research Bulletin*, Vol. 41, No. 1, 2006, pp. 183-190. [doi:10.1016/j.materresbull.2005.07.019](https://doi.org/10.1016/j.materresbull.2005.07.019)
- [11] C. Doroftei, E. Rezlescu, N. Rezlescu and P. D. Popa, "Microstructure and Humidity Sensitive Properties of MgFe<sub>2</sub>O<sub>4</sub> Ferrite with Sn and Mo Substitutions Prepared by Self-combustion Method," *Journal of Optoelectronics and Advanced Materials*, Vol. 8, No. 3, 2006, pp. 1012-1015.
- [12] M. Gateshki, V. Petkov, S. K. Pradhan and T. Vogt, "Structure of Nanocrystalline MgFe<sub>2</sub>O<sub>4</sub> from X-Ray Diffraction, Rietveld and Atomic Pair Distribution Function Analysis," *Journal of Applied Crystallography*, Vol. 38, 2005, pp. 772-779. [doi:10.1107/S0021889805024477](https://doi.org/10.1107/S0021889805024477)
- [13] P. P. Hankare, V. T. Vader, N. M. Patil, S. D. Jadhav, U. B. Sankpal, M. R. Kadam, B. K. Chougule and N. S. Gajbhiye, "Synthesis, Characterization and Studies on Magnetic and Electrical Properties of Mg Ferrite with Cr Substitution," *Materials Chemistry and Physics*, Vol. 113, No. 1, 2009, pp. 233-238. [doi:10.1016/j.matchemphys.2008.07.066](https://doi.org/10.1016/j.matchemphys.2008.07.066)
- [14] A. Sattar, A. H. Wafik and K. M. Kandil, "The Effect of Sintering Temperature on Microhardness and Barkhausen Jumps of Ni and Mg Ferrites," *Journal of Physics D: Applied Physics*, Vol. 29, No. 1, 1996, pp. 25-28. [doi:10.1088/0022-3727/29/1/005](https://doi.org/10.1088/0022-3727/29/1/005)
- [15] M. A. Zinovik and E. V. Zinovik, "Ferrites with Rectangular and Square Hysteresis Loops," *Powder Metal and Metal Ceramics*, Vol. 44, No. 1-2, 2005, pp. 66-74. [doi:10.1007/s11106-005-0059-5](https://doi.org/10.1007/s11106-005-0059-5)